Macromolecules

Article

pubs.acs.org/Macromolecules

Tuning Mechanical and Optoelectrical Properties of Poly(3-hexylthiophene) through Systematic Regioregularity Control

Jin-Seong Kim,[†,#] Jae-Han Kim,[‡,#] Wonho Lee,[†] Hojeong Yu,[§,▽] Hyeong Jun Kim,[†] Inho Song,[§] Minkwan Shin,[⊥] Joon Hak Oh,[§] Unyong Jeong,[∥] Taek-Soo Kim,*[,‡] and Bumjoon J. Kim*[,†]

[†]Department of Chemical and Biomolecular Engineering and [‡]Department of Mechanical Engineering, Korea Advanced Institute of Science and Technology (KAIST), Daejeon 305-701, Korea

[§]Department of Chemical Engineering and [∥]Department of Material Science and Engineering, Pohang University of Science and Technology (POSTECH), Pohang, Gyeongbuk 790-784, Korea

[⊥]Department of Materials Science and Engineering, Yonsei University, Seoul 120-749, Korea

[▽]School of Energy and Chemical Engineering, Ulsan National Institute of Science and Technology (UNIST), Ulsan 689-798, South Korea

Supporting Information

ABSTRACT: While the regioregularity (RR) of conjugated polymers is known to have a strong influence on their inherent properties, systematic study of the RR effect has been limited due to the lack of a synthetic methodology. Herein, we successfully produced a series of poly(3-hexylthiophene)s (P3HTs) having a wide range of RR from 64 to 98%. Incorporation of controlled amounts of head-to-head (H−H) coupled dimer in modified Grignard metathesis polymerization allows a facile tuning of the RR of the P3HTs with comparable molecular weight and low polydispersity. Then, we investigated the effect of RR on structural, electrical, and mechanical properties of P3HTs in which a higher content of H−H regio-defects, namely lower RR, systematically lowered the degree of crystallinity. Although high RR P3HT (98%) had higher charge carrier mobility (1.81×10^{-1} cm^2 V^{-1} s^{-1}), its strong crystallinity induced high brittleness and stiffness, resulting in device failure under a very small strain, as shown in tensile and bending tests. The tensile modulus was reduced significantly from 287 MPa (RR 98%) to 13 MPa (RR 64%), and also the RR 64% P3HT film had much better mechanical resilience with an order of magnitude higher elongation at break than that of the RR 98% polymer. Our findings suggest that the mechanical and electrical properties of conjugated polymers can be systematically tuned by controlling the RR to meet the purposes of various organic electronic applications, i.e., flexible portable devices vs high-performance panels.

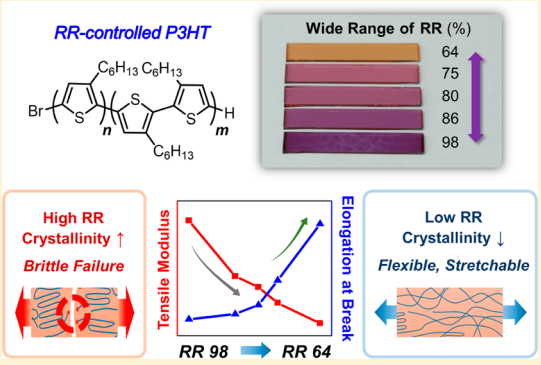

INTRODUCTION

Conjugated polymers have received great attention due to their potential as active components for cost-effective, lightweight, and flexible electronic devices, arising from their solution-based processability.[1−5] Their unique light absorption and charge transport properties are based on the delocalization of π-electrons across the adjacent aligned polymer chains.[6−10] Thus, highly crystalline polymers with well-ordered intermolecular assembly are considered very important for producing efficient electronic devices.[1,11−15] Over the past decade, extensive efforts have been made to increase the degree of intermolecular ordering and crystallinity of the conjugated polymers by tuning the molecular design, such as solubilizing groups[16−19] and backbone structures,[13,15,20−22] with the combination of processing parameters, including thermal[23] or solvent annealing,[24] solvent additives,[25−27] and solution assemblies.[28−30]

However, the excessive crystallization of conjugated polymers has an adverse effect on their processability and mechanical stability, which potentially can cause several problems for their use in organic electronic applications. The strong driving force to form a crystalline phase greatly reduces the solubility of the conjugated polymers, making it difficult to produce a uniform film with cost-effective solution processing techniques.[31,32] Furthermore, for applications such as polymer solar cells, which require a blend of crystalline polymers with fullerenes, higher crystallinity induces a larger extent of phase separation between the two components during subsequent heat exposure upon extended device operation.[33−35] Most importantly, the poor mechanical reliability of highly crystalline polymer films is a significant impediment to the commercialization of organic electronics as portable and flexible devices.[36] The films of highly crystalline polymers have significant brittleness because of the sharp boundary between the crystalline domains. This brittleness leads to the device failure

Received: March 11, 2015
Revised: May 30, 2015
Published: June 16, 2015

DOI: 10.1021/acs.macromol.5b00524
Macromolecules 2015, 48, 4339−4346

Scheme 1. Synthetic Scheme of P3HTs with Different RRs via GRIM Polymerization: Copolymerization of 2,5-Dibromo-3-hexylthiophene (Monomer) and 5′-Bromo-3,4′-dihexyl-5-iodo-[2,2′]-bithiophene (Dimer) with Addition of 1 equiv of LiCl

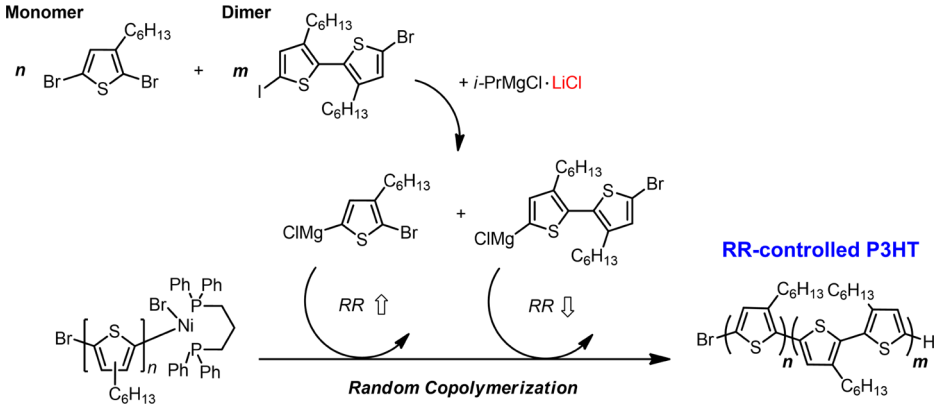

even under a very small amount of strain, thereby seriously decreasing the mechanical reliability and integrity of organic electronics devices.[37−40] Therefore, conjugated polymers must be designed with careful consideration of their mechanical characteristics, such as elasticity and flexibility. However, it has been a great challenge in the development of model polymer systems to establish the structure−property relationship in terms of mechanical properties. In addition, it has been very difficult to perform direct tensile testing of conjugated polymer films with a thickness of less than 100−200 nm, which is the typical thickness of the active layer in organic electronic devices.[41] This, in turn, has induced difficulties in the preparation of specimens without forming wrinkles and cracks for use in testing mechanical properties.

To explore the correlation between the crystallization behavior of conjugated polymers and the resulting device functions, poly(3-hexylthiophene) (P3HT) was selected as a model semicrystalline polymer. Among the various factors that affect the crystalline structure of P3HT, regioregularity (RR), which is defined as a percentage of head-to-tail (H−T) linkage of side chains along the polymer chain, has been identified as a key parameter for determining the primary crystalline structure of polymers[42−44] and their optoelectrical properties.[42,45−48] For example, Kim et al. reported that higher RR P3HT has a stronger tendency to form a highly ordered structure, leading to higher charge carrier mobility and higher optical density.[49] Woo et al. reported that tuning the RR of the polymers is important for optimizing their performance and the thermal stability of polymer solar cells because high RR P3HT induced a larger extent of phase segregation in a blend film with fullerene derivatives under a given thermal annealing condition.[33] Although these studies reported the importance of tuning the RR on enhancing the performances and stabilities of the devices, the results were based on relatively limited control of the RR (i.e., above 86%), and none of the studies addressed the influence of the RR values on the mechanical properties of the polymer thin films. It has been a significant challenge to synthesize P3HT polymers with a wide range of control of their RR values while maintaining comparable number average molecular weights (M_n) and polydispersity indices (PDIs). To date, oxidative polymerization with $FeCl_3$ or palladium-catalyzed cross-coupling polymerization can produce low RR P3HT, but these methods do not allow good control of M_n with low PDI,[50,51] whereas the synthesis of high RR P3HT requires a controlled chain-growth Ni-mediated polymerization that produces relatively low PDI values.[52−56]

In this work, we successfully prepared a series of P3HTs with different RR values from 64 to 98% but with comparable M_n and PDI values. Different RR P3HT polymers were synthesized by the Ni-mediated modified Grignard metathesis (GRIM) polymerization[57] in which 3-hexylthiophene monomer and head-to-head (H−H) coupled 3,4′-dihexyl-2,2′-bithiophene dimer were copolymerized with different feed ratios. We investigated the RR effect on the structural, electrical, and mechanical properties of the P3HTs. Decrease in the RR suppressed the crystalline behavior of the P3HTs and induced changes of the polymer orientation in the thin films, as evidenced by differential scanning calorimetry (DSC) and grazing incident X-ray scattering (GIXS) results. The mechanical and electrical properties were correlated strongly with the RR, which showed mutually conflicting properties in P3HT. Although the lower RR P3HTs had reduced charge carrier mobility in organic thin-film transistors (OTFTs), they had excellent mechanical properties, including low tensile modulus and high elongation, both of which are crucial properties in determining the stretchability and flexibility of the active components in the devices.

RESULTS AND DISCUSSION

For the systematic control of the polymer crystallinity in terms of RR, we synthesized P3HTs with different RR, but with similar M_n (10−20 kg mol^{-1}) and PDI values (1.1−1.4). We used the GRIM polymerization, which commonly yields polythiophenes with the desired M_n and low PDI values,[52,57] but we controlled the feed ratio of the H−H coupled dimer, 5′-bromo-3,4′-dihexyl-5-iodo-[2,2′]-bithiophene,[58] to thiophene monomer (2,5-dibromo-3-hexylthiophene) (Scheme 1). As a result, five different P3HTs were synthesized with different RR of 98, 86, 80, 75, and 64%. For convenience, they were denoted as **RR-98**, **RR-86**, **RR-80**, **RR-75**, and **RR-64**, respectively. The actual RR of the polymers were determined by comparing the integrated area of the peaks at δ 2.78 and δ 2.54 of the ^{1}H NMR spectra (Figure S1), and the M_n and PDI values were determined using size exclusion chromatography (SEC) (Table 1). To obtain precisely controlled M_n value, we added LiCl in the polymerization reaction because it is known to assist the formation of active Grignard monomer and efficiently accelerate polymerization, promoting living characteristics of the polymerization with relatively bulky H−H coupled dimer

DOI: 10.1021/acs.macromol.5b00524
Macromolecules 2015, 48, 4339−4346

Table 1. Characteristics of P3HT Polymers with Different RR Used in This Study

polymer	feed ratio[a] [mole ratio]	RR[b] [% H−T linkages]	M_n[c] [kg mol^{-1}]	PDI[c]
RR-98	100.0:0.0	>98	20.3	1.08
RR-86	94.7:5.3	86	20.8	1.23
RR-80	91.9:8.1	80	13.6	1.42
RR-75	88.9:11.1	75	12.3	1.44
RR-64	82.4:17.6	64	9.2	1.33

[a]Mole ratio between 2,5-dibromo-3-hexylthiophene and 5′-bromo-3,4′-dihexyl-5-iodo-[2,2′]-bithiophene. [b]Percentage of head-to-tail linkages, determined from ^{1}H NMR data (Figure S1). [c]Obtained from SEC calibrated with polystyrene standard.

and thiophene monomer.[55,57,59,60] The polymers were dominantly capped with H/Br end groups, indicative of the chain-growth polymerization with living characteristics (Figure S2). It was observed that the addition of LiCl in the GRIM polymerization was crucial to polymerize low RR P3HTs with desired M_n and PDI values. For example, without the use of LiCl, the highest M_n value of low RR (64%) P3HT that we were able to achieve through several tries remained low as M_n < 2.7 kg mol^{-1}, with high PDI values (>1.5), which shows a stark contrast to the values of **RR-64** polymers synthesized with the presence of LiCl. It is noted that this is the first reported synthesis of P3HTs with a wide range of RR via GRIM polymerization; thus, this study can serve as a guideline for other RR studies.

The quantitative effects of the RR on the crystallinity and thermal properties of the P3HT series were examined using DSC measurements. Figure 1a shows the heating and cooling thermograms (second cycle) of the **RR-98**, **RR-86**, **RR-80**, **RR-75**, and **RR-64**, and Table S1 summarizes their thermal characteristics. In the heating cycle, **RR-98** had the highest melting temperature (T_m) of 231 °C, which agreed well with the previously reported T_m values for P3HTs with high values of RR.[33,42] The T_m values of **RR-86**, **RR-80**, and **RR-75** decreased progressively to 214, 197, and 184 °C, respectively. The melting peak disappeared for **RR-64** P3HT (Figure 1a, left). In the cooling cycle, a similar trend was observed in the crystallization temperatures (T_c). The T_c values of **RR-98**, **RR-86**, **RR-80**, and **RR-75** P3HT polymers were remarkably reduced from 200, 182, 171, to 152 °C, respectively (Figure 1a, right). Again, the crystallization peak for **RR-64** was almost negligible. These strong decreasing trends in the T_m and T_c values indicated that the decrease of the RR of P3HT induced a remarkable decrease in the interchain interaction and suppressed the formation of crystalline structures. In addition, the glass transition behavior of the amorphous region of P3HT was irrelevant to the changes of the RR, as evidenced by the fact that similar glass transition temperatures (T_g), in the range of 0−10 °C, were observed for different RR P3HTs (Figure S3). For a quantitative comparison of the thermal properties, the melting enthalpy (ΔH_m) was compared for the P3HT series, and their degrees of crystallinity were calculated by comparing their ΔH_m value with the melting enthalpy of an ideal P3HT crystallite (ΔH_m° = 37 J g^{-1}).[42] Accordingly, the degrees of crystallinity were calculated to be 48.4 (**RR-98**), 30.6 (**RR-86**), 22.4 (**RR-80**), 15.8 (**RR-75**), and approximately 0% (**RR-64**) (Figure 1b). As the RR decreased, the degree of crystallinity also decreased linearly, indicating that the incorporation of regio-defects in P3HT disturbed the formation of crystalline

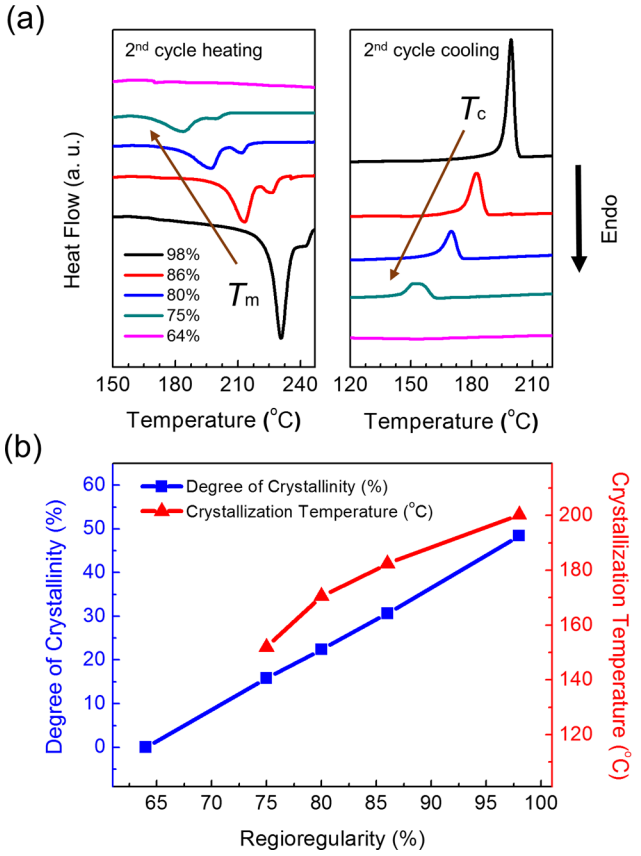

Figure 1. (a) DSC second heating and cooling cycles at a rate of 10 °C min^{-1}. Both the melting temperature (T_m) and crystallization temperature (T_c) of the P3HT polymers decreased as the RR decreased. (b) T_c and the degree of crystallinity as a function of RR.

structures. Thus, the crystallinity of P3HT can be effectively controlled by tuning the RR, and even the small change in RR value resulting from the incorporation of 5% of the H−H dimer produced significant changes in the thermal properties and crystallinity.

The structural properties of the RR-controlled P3HT polymers in thin films were compared by GIXS measurements (Figure 2). All the samples were prepared under identical conditions. The polymers in chlorobenzene solutions were spin-coated to produce 100 nm thick films on the silicon substrates. The **RR-98** exhibited highly ordered (h00) scattering peaks that corresponded to the lamellar stacks in the out-of-plane direction (q_z) and the (010) peak that corresponded to the $\pi-\pi$ stacking in the in-plane direction (q_{xy}), indicating that the polymer films had a well-organized structure with edge-on geometry (Figure S4). These results were in excellent agreement with those reported for high RR P3HT.[46,61] As the RR decreased, the intensities of the peaks became much weaker, indicating that the degree of crystalline ordering in the P3HT polymers was decreased significantly. For **RR-64**, the $\pi-\pi$ stacking peaks almost disappeared. Interestingly, the RR affected the orientation of the P3HT stacks in the thin film. Higher RR P3HT polymers had a greater preference for the "edge-on" molecular orientation (Figure 2). For quantitative analysis, the intensity ratio of the out-of-plane to the in-plane $\pi-\pi$ stacking peaks (I_{op}/I_{ip}) was calculated,[18] confirming the changes in the P3HT orientation in thin films in terms of RR (Table S2). According to recent studies of Osaka

DOI: 10.1021/acs.macromol.5b00524
Macromolecules 2015, 48, 4339−4346

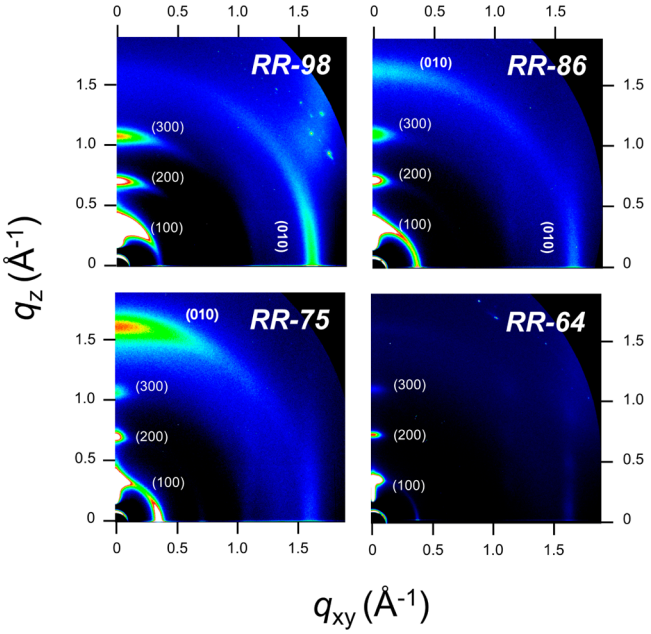

Figure 2. GIXS 2D images of as-spun-cast P3HT films.

et al. and Abdulrahman et al., the decrease of planarity from introducing nonlinear side chains led conjugated polymer crystallites preferentially "face-on" orientation in thin films for the same backbone structure.[18,62] Likewise, we speculate that the regio-defects in low RR P3HT reduce the planarity of the polymer and disturb the formation of "edge-on" oriented crystallites. Since the RR determines the crystalline behavior of the P3HT polymers and also affects the polymer orientation in thin film, tuning the RR can provide a model system for investigation of the correlation between the crystalline behavior of the polymers and their other properties including mechanical and electrical properties, device performances, and stabilities.

We also investigated the effect of RR on the optical and electrochemical properties of P3HT. Figure S5 shows the normalized absorption spectra of the **RR-98**, **RR-86**, **RR-80**, **RR-75**, and **RR-64** in diluted chlorobenzene solution and in thin film, and the results are summarized in Table S3. In the solution, all of the RR-controlled P3HTs exhibited similarly shaped absorption curves, but the maximum absorption peaks (λ_{max}) were blue-shifted slightly from 457 (**RR-98**) to 441 nm (**RR-64**). The RR had much greater influence on the absorption in thin films; the λ_{max} values were considerably blue-shifted from 557 nm (**RR-98**) to 496 nm (**RR-64**), and the vibronic peaks (A_{0-1} and A_{0-0}) were significantly decreased as the RR decreased. Therefore, the optical bandgaps (E_g^{opt}) of the P3HTs were increased gradually from 1.88 eV (**RR-98**) to 1.94 eV (**RR-64**). The change of the planarity of the P3HTs also affected their effective conjugation length and the packing structures, influencing on the highest occupied molecular orbital (HOMO) and the lowest unoccupied molecular orbital (LUMO) levels of the P3HT. The electrochemical properties of the RR-controlled P3HTs were measured using cyclic voltammetry (CV), and their HOMO and LUMO are summarized in Table S3. As the RR decreased, the HOMO decreased progressively from −5.16 eV (**RR-98**) to −5.59 eV (**RR-64**) and the LUMO decreased from −3.28 eV (**RR-98**) to −3.65 eV (**RR-64**). Consequently, controlling the RR enabled the tuning of the optical and electrochemical properties of the conjugated polymers.[63]

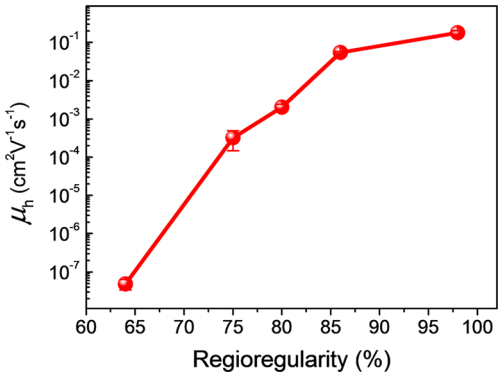

Figure 3. Charge carrier mobility of P3HT polymers as a function of RR determined from transfer curves at V_{DS} = −100 V (bottom-gate, top-contact configuration with OTS-treated 300 nm SiO_2/Si wafer).

To examine the effects of the RR on the electrical properties of the P3HTs, we fabricated bottom-gate, top-contact OTFT devices based on a series of P3HT polymers (Figure 3). All of the P3HTs having different RR were drop-casted onto an *n*-octadecyltrimethoxysilane (OTS)-coated SiO_2/Si substrate from the chloroform solution, and then thermal annealing was applied at 150 °C. Figure S6 shows the transfer characteristics of OTFTs based on the drop-cast P3HT thin films, and Table S4 summarizes their electrical performances. The average hole mobilities (μ_h) of **RR-98**, **RR-86**, **RR-80**, **RR-75**, and **RR-64** were observed to be 1.81×10^{-1}, 5.47×10^{-2}, 2.03×10^{-3}, 3.22×10^{-4}, and 4.84×10^{-8} cm^2 V^{-1} s^{-1}, respectively (Figure 3). The insertion of regio-defects into the polymer backbone reduced the effective conjugation length of each polymer chain as well as the intermolecular assembly by $\pi-\pi$ interactions, resulting in the decrease of the ordered-crystalline domain and the reduction in the μ_h value. Especially, **RR-64**, which contained the highest ratio of regio-defects, exhibited a drastic decrease of μ_h value than **RR-75**. This is consistent with the GIXS results of the **RR-64** polymers. Their $\pi-\pi$ stacking peaks almost disappeared, and the polymers had less preference for the "edge-on" molecular orientation, which is not suitable for charge transport between the source and drain electrodes in OTFTs.

In order to measure the mechanical properties of P3HT thin films with respect to RR, pseudo-free-standing tensile tests were performed.[64] Direct tensile testing of conjugated polymers at the nanoscale has been considered very difficult due to the demanding specimen fabrication and manipulation. In contrast, for the pseudo-free-standing tensile tests, easy handling and almost frictionless sliding of the P3HT thin films can be achieved on the water surface without any significant damage or wrinkling of the specimens due to the high surface tension and low viscosity of water. In this way, we were able to measure the intrinsic mechanical properties of P3HT thin films quantitatively without any substrate effects, complex calculations, or assumptions. Figure 4a shows the P3HT thin films fabricated on poly(3,4-ethylenedioxythiophene)−poly(styrenesulfonate) (PEDOT:PSS)/glass substrate with different RR (**RR-98**, **RR-86**, **RR-80**, **RR-75**, and **RR-64**). The thickness of each specimen was approximately 100 nm, which was measured by surface profiler (Tencor-Alpha Step IQ). Clear differences in the light absorption properties of the different RR P3HT polymers were visualized by the contrast in the color of their thin films in terms of RR. By dissolving the PEDOT:PSS layer at deionized water surface, the P3HT thin films were easily

DOI: 10.1021/acs.macromol.5b00524
Macromolecules 2015, 48, 4339−4346

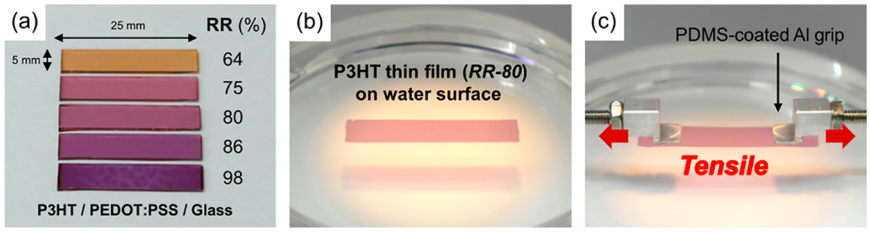

Figure 4. (a) P3HT polymer thin films with different RR, fabricated on PEDOT:PSS/glass substrate. (b) P3HT thin film floating on the water surface. (c) Tensile testing of the P3HT polymer thin films on the water surface. Tensile testing was performed with a strain rate of 0.3×10^{-3} s^{-1}.

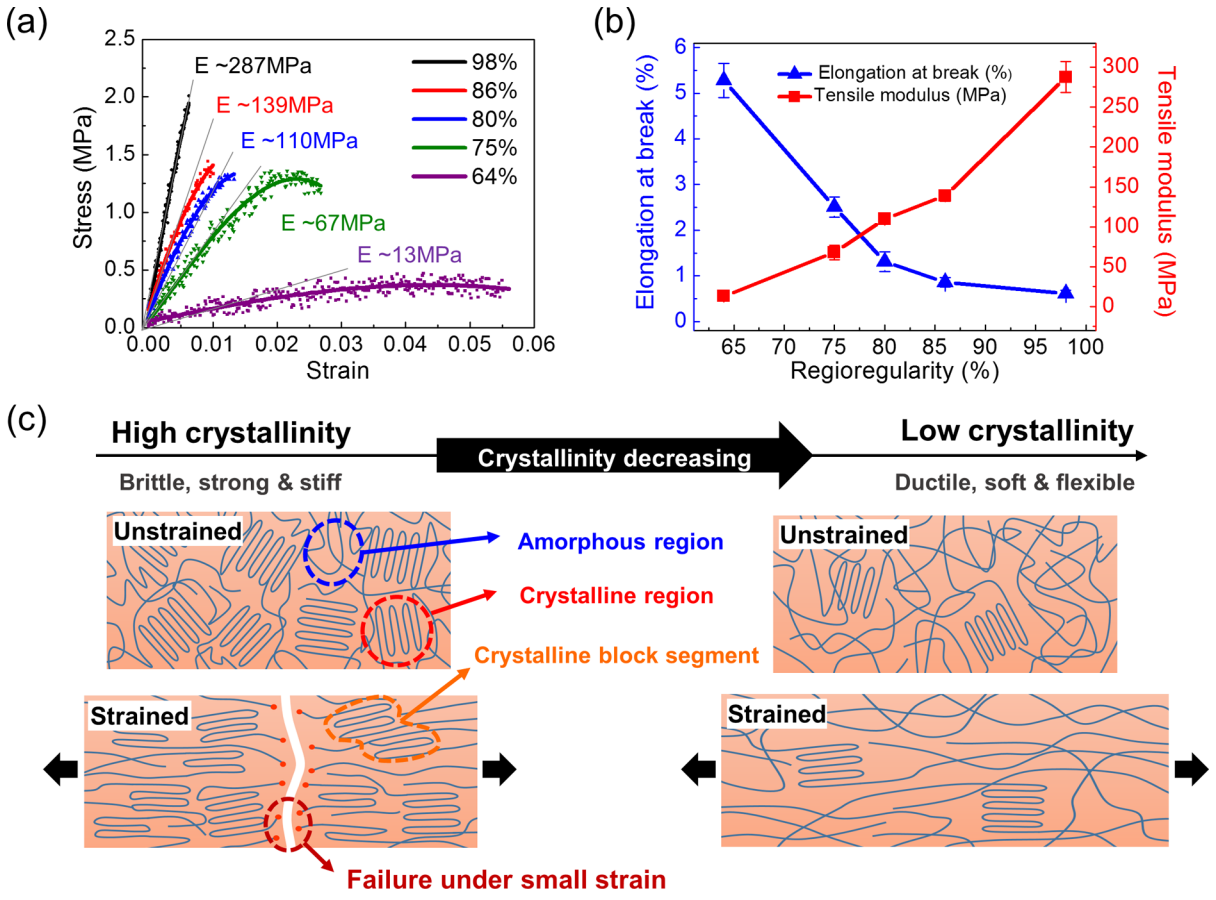

Figure 5. Mechanical properties and deformation mechanism of P3HT polymer thin films as a function of RR. (a) Stress−strain curves of the P3HT thin films with the RR of 98, 86, 80, 75, and 64%. (b) Tensile modulus and elongation at break of the P3HT thin films. (c) Strain-evolved deformation mechanism of conjugated polymer thin films under tensile strain with respect to the degree of crystallinity.

separated from the glass substrate, and subsequently, the thin films floated on the water surface as depicted in Figure 4b. In order to manipulate the specimens on the water surface, polydimethylsiloxane (PDMS)-coated Al grips were attached on the film surface using van der Waals adhesion. Then, the tensile test was performed by applying a tensile force using a linear stage, as shown in Figure 4c and Figure S7.

Figure 5a shows the representative stress−strain curves of the P3HT thin films that measure their tensile modulus and elongation at break. Interestingly, the mechanical properties of P3HTs were significantly changed with respect to the RR. The measured tensile moduli of the **RR-98**, **RR-86**, **RR-80**, **RR-75**, and **RR-64** thin films were 287 ± 19, 139 ± 7, 110 ± 5, 68 ± 9, and 13 ± 2 MPa, respectively (Figure 5b). Each value represents the average of five specimens tested. The tensile modulus of 287 ± 19 MPa for **RR-98** film was in good agreement with previously reported values for P3HT films, i.e., 250 ± 60 MPa[38] and 220 ± 30 MPa.[39] The tensile modulus gradually decreased from 287 MPa for **RR-98** to 13 MPa for **RR-64**. The tensile modulus (13 MPa) for **RR-64** was especially low, even lower than the tensile modulus values reported to date for other conjugated polymer films.[36] The elongation at break of the P3HT thin films was also obtained, as presented in Figure 5b. As RR decreased, the elongation at break increased significantly to 5.3% for the **RR-64** film, which was an order of magnitude higher than the elongation at break of the **RR-98** P3HT (0.6%). This also leads to an increase in toughness, and the enhancement in the elongation and toughness of the polymers would provide improved mechanical ability to withstand deformation.

The significant differences in the mechanical properties of the P3HT thin films as a function of the RR was primarily attributed to the degree of crystallinity.[65,66] Highly crystalline **RR-98** P3HT polymer films were much stiffer and more brittle

DOI: 10.1021/acs.macromol.5b00524
Macromolecules 2015, 48, 4339−4346

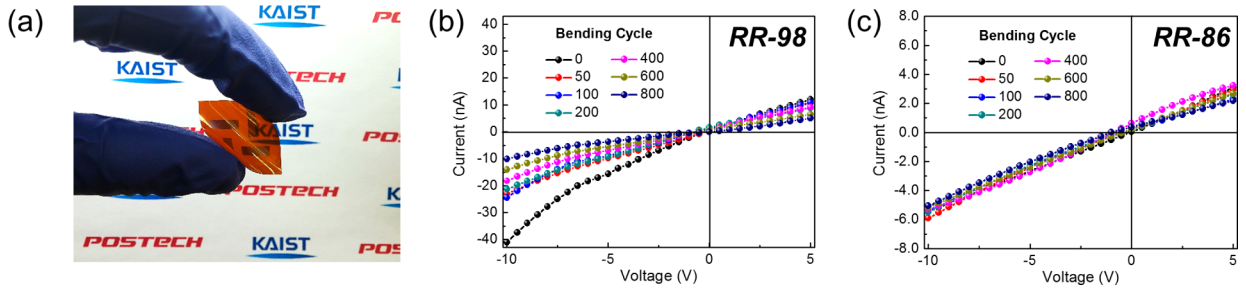

Figure 6. Mechanical stability of P3HT thin films with different RRs against bending tests. (a) Photograph of P3HT thin film on PI substrate under bending strain. Current−voltage (I−V) curves of (b) **RR-98** and (c) **RR-86** P3HT thin films after bending tests with cycle numbers from 0 to 800.

than the lower RR P3HT samples that had lower crystallinity. Based on the results of the mechanical tests, the deformation mechanism for high and low crystalline P3HT thin films is schematically illustrated in Figure 5c. For the higher RR, more polymer chains are close-packed in an ordered arrangement as shown in Figure 5c, left. This improved molecular packing in P3HT crystalline region extensively increases the density of secondary intermolecular bonding through van der Waals and π−π interactions. Since the crystalline region inhibits chain deformation and exhibits a high resistance to elastic deformation, the strengths of semicrystalline polymers should be enhanced, resulting in a higher tensile modulus as the RR increased. However, a more brittle behavior was observed for higher RR P3HT. The cracks or failure of the polymer films occurred easily even under small mechanical deformation, resulting in smaller elongation at break in the higher RR P3HTs. In contrast, for the lower RR P3HT, the regio-defects interrupted the formation of crystalline structures, which led to increased amorphous regions due to the steric hindrance within the polymer chain. Accordingly, when tensile strain was applied to the lower RR P3HT thin films, the polymer chains in the amorphous regions easily aligned and were extended under relatively low applied force along the strain axis, as described in Figure 5c, right. Subsequently, this resulted in the reduced tensile modulus and increased elongation, both of which can provide great advantages for the applications in flexible and stretchable electronics with enhanced mechanical reliabilities.

To examine the stability of the electrical performances of the P3HT thin films against external mechanical deformation, their current−voltage (I−V) characteristics were measured after multiple cycles of bending strain.[67,68] For the bending tests, the P3HT thin films were spin-coated on a polyimide (PI) film with a thickness of 80 μm. Then, a Au layer (70 nm) was thermally evaporated as the electrode (Figure 6a). The I−V characteristics of the P3HT thin films were measured after different bending cycles from 0 to 800 with 1.5 mm of bending radius (R). The bending test results showed that the current values of **RR-98** thin film were radically decreased during the first 50 cycles and significantly degraded by approximately 75% compared to the initial value as increasing the bending cycles (Figure 6b). In stark contrast, the current value of **RR-86** thin film was almost maintained (i.e., decreased by only 7%) even after 800 bending cycles (Figure 6c). Although the higher RR P3HT had better electrical properties initially, the cracks and failures of the thin film induced drastic degradation of electrical performances under deformations due to its brittle characteristics. In contrast, lower RR P3HT films showed excellent tolerance against the external strains with stable electrical performance. Therefore, optimizing the RR of P3HT can be an effective approach for ensuring the mechanical stability of high-performance organic electronics.

CONCLUSIONS

A series of P3HTs with a wide range of RR were prepared, and the RR effects on their mechanical and electrical properties were investigated. The facile tuning of RR from 64 to 98% was successfully achieved by copolymerization of different amounts of the H−H coupled dimers using modified GRIM polymerization. GIXS and DSC analyses demonstrated that the decrease in the RR caused the distortion of packing structures and subsequently lowered the degree of crystallinity of the P3HTs. The changes in the packing structure and the crystalline behaviors of the P3HTs as a function of RR significantly affect their mechanical and electrical properties. Although the lower RR P3HTs had reduced electrical performance, it had great advantages with respect to the mechanical properties: decreased tensile modulus with increased elongation for enhanced mechanical stability. Therefore, our model study provides important guidelines for the design of the electroactive polymers required for flexible and stretchable electronic applications, especially for optimizing the mechanical and electrical performances.

EXPERIMENTAL SECTION

General Synthesis of RR-Controlled P3HTs. 2,5-Dibromo-3-hexylthiophene (2.82 mmol, 0.92 g) and 5′-bromo-3,4′-dihexyl-5-iodo-[2,2′]-bithiophene (0.16 mmol, 0.09 g) were mixed in a flask under a nitrogen atmosphere, and then, 20 mL of dry THF was added into the flask. After stirring at 0 °C, isopropylmagnesium chloride−lithium chloride complex solution (1.3 M solution in THF, 2.20 mL, 1.72 mmol) was added, and the mixture was stirred for 1 h. Afterward, a Ni(dppp)Cl_2 suspension (0.09 mmol, 0.05 g) in dry THF (0.5 mL) was added to the mixture to initiate polymerization. After stirring for 1 h at room temperature, HCl aqueous solution (1 M, 1 mL) was added for the termination, and the polymers were precipitated in methanol after 10 min. To remove any impurities, the crude polymers were purified via Soxhlet extraction with methanol, acetone, hexane, and chloroform. The chloroform fraction was precipitated in methanol and filtered followed by drying under the vacuum (247 mg, yield: 50%).

Differential Scanning Calorimetry (DSC). DSC curves were obtained from a TA Instruments DSC Q200. The polymer samples (~5 mg) were heated from 25 to 300 °C at a heating rate of 10 °C min^{-1} and then cooled down at a rate of 10 °C min^{-1} under an inert atmosphere. The scans were performed twice for each sample.

Grazing-Incidence X-ray Scattering (GIXS). The thin films of polymers (~100 nm) were prepared by spin-coating on Si-wafers from chlorobenzene solutions. GIXS measurements were obtained from beamline 3C in the Pohang Accelerator Laboratory (South Korea) at a wavelength of 1.1010 Å. The incidence angle of the beam was set between the critical angles of the polymer films and the silicon substrate (in the range 0.15°−0.18°). The X-ray beams scattered by

DOI: 10.1021/acs.macromol.5b00524
Macromolecules 2015, 48, 4339−4346

the films were collected by two-dimensional CCD detector at a sample-to-detector distance of 0.2 m.

OTFT Device Fabrication and Measurements. OTFT devices with bottom-gate top-contact configuration were prepared to characterize the electrical performance of P3HTs. A highly n-doped (100) Si wafer (<0.004 Ω·cm) with a thermally grown SiO_2 (300 nm, C_i = 10 nF cm^{-2}) was utilized as the gate and dielectric. The surface of the SiO_2 was modified with *n*-OTS monolayer as previously reported.[69,70] 3 mM of OTS solution in trichloroethylene was spin-coated on the piranha-cleaned wafer at 3000 rpm for 30 s. Then, the wafer was exposed to ammonia vapor for 12 h to facilitate the formation of OTS layer, followed by sonication cleaning, sequential washing, and drying. The contact angle on the hydrophobic OTS-modified wafer with water droplet was >106°. The series of P3HTs were dissolved in chloroform (4 mg mL^{-1}), and the film was drop-cast onto the OTS-treated SiO_2/Si substrates and then annealed on a hot plate at 150 °C for 30 min under N_2 atmosphere. Au electrodes (40 nm) were thermally evaporated onto the film to form source and drain electrodes with a channel length (L) of ∼50 μm and a channel width (W) of ∼1000 μm using a shadow mask. The electrical performance was measured in a N_2-filled glovebox using a Keithley 4200 semiconductor parametric analyzer. The field-effect mobility was calculated in the saturation regime using the equation

$$I_D = \frac{W}{2L}\mu C_i(V_{GS} - V_T)^2$$

where I_D is the drain-to-source current, W and L are the semiconductor channel width and length, respectively, μ is the mobility, and V_{GS} and V_T are the gate voltage and threshold voltage, respectively.

Pseudo-Free-Standing Tensile Test of P3HT Thin Films. For the tensile testing of P3HT thin films, P3HT was spin-coated (∼100 nm) onto the PEDOT:PSS/glass substrate. After the film deposition, the P3HT/PEDOT:PSS/glass specimen is cut into bar-type tensile specimens with the size of 25 × 5 mm. In order to float the P3HT thin film on the surface of the water, the DI water was penetrated into dissolve PEDOT:PSS layer. Subsequently, the PEDOT:PSS layer was removed and the P3HT film was separated from the glass substrate. This process resulted the P3HT thin film afloat on the water surface. PDMS-coated Al grips were used to manipulate the thin film on the water surface. The tensile force was applied to the specimen using a linear stage with strain rate of 0.3 × 10^{-3} s^{-1}, and all tensile tests were performed in a lab air environment at ∼21 °C. During the tensile test, load and strain data were continuously obtained by a high-resolution load cell (LTS-10GA, KYOWA, Japan) and a digital image correlation (DIC) device, respectively. A photograph of the pseudo-free-standing tensile testing system is shown in the Supporting Information. The system mainly consists of a load cell, a linear actuator, and a DIC camera on an antivibration table.

■ ASSOCIATED CONTENT

Supporting Information

Detailed experimental procedure and additional characterization data. The Supporting Information is available free of charge on the ACS Publications website at DOI: 10.1021/acs.macromol.5b00524.

■ AUTHOR INFORMATION

Corresponding Authors

*E-mail bumjoonkim@kaist.ac.kr (B.J.K.).
*E-mail tskim1@kaist.ac.kr (T.-S.K.).

Author Contributions

#J.-S.K. and J.-H.K. contributed equally to this work.

Notes

The authors declare no competing financial interest.

■ ACKNOWLEDGMENTS

This research was supported by the National Research Foundation Grant (2012R1A1A2A10041283, 2012R1A1A1006072) and by the Global Frontier R&D Program on Center for Multiscale Energy System (2012M3A6A7055540), funded by the Korean Government. Authors also acknowledge the Research Project of the KAIST High-Risk High-Return for the financial support.

■ REFERENCES

(1) Thompson, B. C.; Frechet, J. M. J. *Angew. Chem., Int. Ed.* **2008**, *47* (1), 58−77.
(2) Torsi, L.; Magliulo, M.; Manoli, K.; Palazzo, G. *Chem. Soc. Rev.* **2013**, *42* (22), 8612−8628.
(3) Arias, A. C.; MacKenzie, J. D.; McCulloch, I.; Rivnay, J.; Salleo, A. *Chem. Rev.* **2010**, *110* (1), 3−24.
(4) D'Andrade, B. W.; Forrest, S. R. *Adv. Mater.* **2004**, *16* (18), 1585−1595.
(5) Schwartz, G.; Tee, B. C. K.; Mei, J. G.; Appleton, A. L.; Kim, D. H.; Wang, H. L.; Bao, Z. N. *Nat. Commun.* **2013**, *4*, 1859.
(6) Heeger, A. J.; Kivelson, S.; Schrieffer, J. R.; Su, W. P. *Rev. Mod. Phys.* **1988**, *60* (3), 781−850.
(7) Kraft, A.; Grimsdale, A. C.; Holmes, A. B. *Angew. Chem., Int. Ed.* **1998**, *37* (4), 402−428.
(8) Bredas, J. L.; Beljonne, D.; Coropceanu, V.; Cornil, J. *Chem. Rev.* **2004**, *104* (11), 4971−5003.
(9) Zaumseil, J.; Sirringhaus, H. *Chem. Rev.* **2007**, *107* (4), 1296−1323.
(10) Coakley, K. M.; McGehee, M. D. *Chem. Mater.* **2004**, *16* (23), 4533−4542.
(11) Lee, W.; Kim, G. H.; Ko, S. J.; Yum, S.; Hwang, S.; Cho, S.; Shin, Y. H.; Kim, J. Y.; Woo, H. Y. *Macromolecules* **2014**, *47* (5), 1604−1612.
(12) Brown, P. J.; Thomas, D. S.; Kohler, A.; Wilson, J. S.; Kim, J. S.; Ramsdale, C. M.; Sirringhaus, H.; Friend, R. H. *Phys. Rev. B* **2003**, *67* (6), 064203.
(13) Kim, K.-H.; Park, S.; Yu, H.; Kang, H.; Song, I.; Oh, J. H.; Kim, B. J. *Chem. Mater.* **2014**, *26* (24), 6963−6970.
(14) Cheng, Y. J.; Yang, S. H.; Hsu, C. S. *Chem. Rev.* **2009**, *109* (11), 5868−5923.
(15) Nguyen, T. L.; Choi, H.; Ko, S. J.; Uddin, M. A.; Walker, B.; Yum, S.; Jeong, J. E.; Yun, M. H.; Shin, T. J.; Hwang, S.; Kim, J. Y.; Woo, H. Y. *Energy Environ. Sci.* **2014**, *7* (9), 3040−3051.
(16) Ho, V.; Boudouris, B. W.; Segalman, R. A. *Macromolecules* **2010**, *43* (19), 7895−7899.
(17) Cho, C. H.; Kim, H. J.; Kang, H.; Shin, T. J.; Kim, B. J. *J. Mater. Chem.* **2012**, *22* (28), 14236−14245.
(18) Osaka, I.; Saito, M.; Koganezawa, T.; Takimiya, K. *Adv. Mater.* **2014**, *26* (2), 331−338.
(19) Cabanetos, C.; El Labban, A.; Bartelt, J. A.; Douglas, J. D.; Mateker, W. R.; Frechet, J. M. J.; McGehee, M. D.; Beaujuge, P. M. *J. Am. Chem. Soc.* **2013**, *135* (12), 4656−4659.
(20) Cho, H. H.; Kang, T. E.; Kim, K. H.; Kang, H.; Kim, H. J.; Kim, B. J. *Macromolecules* **2012**, *45* (16), 6415−6423.
(21) Zhou, H. X.; Yang, L. Q.; You, W. *Macromolecules* **2012**, *45* (2), 607−632.
(22) Li, Y. *Acc. Chem. Res.* **2012**, *45* (5), 723−733.
(23) Ma, W. L.; Yang, C. Y.; Gong, X.; Lee, K.; Heeger, A. J. *Adv. Funct. Mater.* **2005**, *15* (10), 1617−1622.
(24) Li, G.; Yao, Y.; Yang, H.; Shrotriya, V.; Yang, G.; Yang, Y. *Adv. Funct. Mater.* **2007**, *17* (10), 1636−1644.
(25) Lee, J. K.; Ma, W. L.; Brabec, C. J.; Yuen, J.; Moon, J. S.; Kim, J. Y.; Lee, K.; Bazan, G. C.; Heeger, A. J. *J. Am. Chem. Soc.* **2008**, *130* (11), 3619−3623.
(26) Hoven, C. V.; Dang, X. D.; Coffin, R. C.; Peet, J.; Nguyen, T. Q.; Bazan, G. C. *Adv. Mater.* **2010**, *22* (8), E63−E66.

DOI: 10.1021/acs.macromol.5b00524
Macromolecules 2015, 48, 4339−4346

(27) Kang, H.; Uddin, M. A.; Lee, C.; Kim, K.-H.; Nguyen, T. L.; Lee, W.; Li, Y.; Wang, C.; Woo, H. Y.; Kim, B. J. *J. Am. Chem. Soc.* **2015**, *137* (6), 2359−2365.
(28) Clark, J.; Chang, J. F.; Spano, F. C.; Friend, R. H.; Silva, C. *Appl. Phys. Lett.* **2009**, *94* (16), 163306.
(29) Xin, H.; Kim, F. S.; Jenekhe, S. A. *J. Am. Chem. Soc.* **2008**, *130* (16), 5424−5425.
(30) Kim, Y. J.; Cho, C. H.; Paek, K.; Jo, M.; Park, M. K.; Lee, N. E.; Kim, Y. J.; Kim, B. J.; Lee, E. *J. Am. Chem. Soc.* **2014**, *136* (7), 2767−2774.
(31) Hiorns, R. C.; De Bettignies, R.; Leroy, J.; Bailly, S.; Firon, M.; Sentein, C.; Khoukh, A.; Preud'homme, H.; Dagron-Lartigau, C. *Adv. Funct. Mater.* **2006**, *16* (17), 2263−2273.
(32) Yiu, A. T.; Beaujuge, P. M.; Lee, O. P.; Woo, C. H.; Toney, M. F.; Frechet, J. M. J. *J. Am. Chem. Soc.* **2012**, *134* (4), 2180−2185.
(33) Woo, C. H.; Thompson, B. C.; Kim, B. J.; Toney, M. F.; Frechet, J. M. J. *J. Am. Chem. Soc.* **2008**, *130* (48), 16324−16329.
(34) Kim, H. J.; Kim, J.-H.; Ryu, J.-H.; Kim, Y.; Kang, H.; Lee, W. B.; Kim, T.-S.; Kim, B. J. *ACS Nano* **2014**, *8* (10), 10461−10470.
(35) Kim, H. J.; Han, A. R.; Cho, C. H.; Kang, H.; Cho, H. H.; Lee, M. Y.; Frechet, J. M. J.; Oh, J. H.; Kim, B. J. *Chem. Mater.* **2012**, *24* (1), 215−221.
(36) Savagatrup, S.; Printz, A. D.; O'Connor, T. F.; Zaretski, A. V.; Rodriquez, D.; Sawyer, E. J.; Rajan, K. M.; Acosta, R. I.; Root, S. E.; Lipomi, D. J. *Energy Environ. Sci.* **2015**, *8*, 55−80.
(37) Reddy, C. M.; Padmanabhan, K. A.; Desiraju, G. R. *Cryst. Growth Des.* **2006**, *6* (12), 2720−2731.
(38) O'Connor, B.; Chan, E. P.; Chan, C.; Conrad, B. R.; Richter, L. J.; Kline, R. J.; Heeney, M.; McCulloch, I.; Soles, C. L.; DeLongchamp, D. M. *ACS Nano* **2010**, *4* (12), 7538−7544.
(39) Awartani, O.; Lemanski, B. I.; Ro, H. W.; Richter, L. J.; DeLongchamp, D. M.; O'Connor, B. T. *Adv. Energy Mater.* **2013**, *3* (3), 399−406.
(40) Savagatrup, S.; Makaram, A. S.; Burke, D. J.; Lipomi, D. J. *Adv. Funct. Mater.* **2014**, *24* (8), 1169−1181.
(41) Li, G.; Shrotriya, V.; Yao, Y.; Yang, Y. *J. Appl. Phys.* **2005**, *98* (4), 043704.
(42) Kohn, P.; Huettner, S.; Komber, H.; Senkovskyy, V.; Tkachov, R.; Kiriy, A.; Friend, R. H.; Steiner, U.; Huck, W. T. S.; Sommer, J. U.; Sommer, M. *J. Am. Chem. Soc.* **2012**, *134* (10), 4790−4805.
(43) Snyder, C. R.; Henry, J. S.; DeLongchamp, D. M. *Macromolecules* **2011**, *44* (18), 7088−7091.
(44) Willot, P.; Steverlynck, J.; Moerman, D.; Leclere, P.; Lazzaroni, R.; Koeckelberghs, G. *Polym. Chem.* **2013**, *4* (9), 2662−2671.
(45) Jiang, X. M.; Osterbacka, R.; Korovyanko, O.; An, C. P.; Horovitz, B.; Janssen, R. A. J.; Vardeny, Z. V. *Adv. Funct. Mater.* **2002**, *12* (9), 587−597.
(46) Sirringhaus, H.; Brown, P. J.; Friend, R. H.; Nielsen, M. M.; Bechgaard, K.; Langeveld-Voss, B. M. W.; Spiering, A. J. H.; Janssen, R. A. J.; Meijer, E. W.; Herwig, P.; de Leeuw, D. M. *Nature* **1999**, *401* (6754), 685−688.
(47) Chen, T. A.; Rieke, R. D. *Synth. Met.* **1993**, *60* (2), 175−177.
(48) Mauer, R.; Kastler, M.; Laquai, F. *Adv. Funct. Mater.* **2010**, *20* (13), 2085−2092.
(49) Kim, Y.; Cook, S.; Tuladhar, S. M.; Choulis, S. A.; Nelson, J.; Durrant, J. R.; Bradley, D. D. C.; Giles, M.; Mcculloch, I.; Ha, C. S.; Ree, M. *Nat. Mater.* **2006**, *5* (3), 197−203.
(50) Wang, Q. F.; Takita, R.; Kikuzaki, Y.; Ozawa, F. *J. Am. Chem. Soc.* **2010**, *132* (33), 11420−11421.
(51) McCullough, R. D. *Adv. Mater.* **1998**, *10* (2), 93−116.
(52) Miyakoshi, R.; Yokoyama, A.; Yokozawa, T. *J. Am. Chem. Soc.* **2005**, *127* (49), 17542−17547.
(53) Tkachov, R.; Senkovskyy, V.; Komber, H.; Sommer, J. U.; Kiriy, A. *J. Am. Chem. Soc.* **2010**, *132* (22), 7803−7810.
(54) Loewe, R. S.; Khersonsky, S. M.; McCullough, R. D. *Adv. Mater.* **1999**, *11* (3), 250−253.
(55) Lohwasser, R. H.; Thelakkat, M. *Macromolecules* **2011**, *44* (9), 3388−3397.
(56) Bronstein, H. A.; Luscombe, C. K. *J. Am. Chem. Soc.* **2009**, *131* (36), 12894−12895.
(57) Iovu, M. C.; Sheina, E. E.; Gil, R. R.; McCullough, R. D. *Macromolecules* **2005**, *38* (21), 8649−8656.
(58) Beryozkina, T.; Senkovskyy, V.; Kaul, E.; Kiriy, A. *Macromolecules* **2008**, *41* (21), 7817−7823.
(59) Stefan, M. C.; Javier, A. E.; Osaka, I.; McCullough, R. D. *Macromolecules* **2009**, *42* (1), 30−32.
(60) Miyakoshi, R.; Shimono, K.; Yokoyama, A.; Yokozawa, T. *J. Am. Chem. Soc.* **2006**, *128* (50), 16012−16013.
(61) Johnston, D. E.; Yager, K. G.; Hlaing, H.; Lu, X. H.; Ocko, B. M.; Black, C. T. *ACS Nano* **2014**, *8* (1), 243−249.
(62) El Labban, A.; Warnan, J.; Cabanetos, C.; Ratel, O.; Tassone, C.; Toney, M. F.; Beaujuge, P. M. *ACS Appl. Mater. Interfaces* **2014**, *6* (22), 19477−19481.
(63) Spano, F. C. *J. Chem. Phys.* **2005**, *122* (23), 234701.
(64) Kim, J. H.; Nizami, A.; Hwangbo, Y.; Jang, B.; Lee, H. J.; Woo, C. S.; Hyun, S.; Kim, T. S. *Nat. Commun.* **2013**, *4*, 2520.
(65) Landel, R. F.; Nielsen, L. E. *Mechanical Properties of Polymers and Composites*; CRC Press: Boca Raton, FL, 1993.
(66) Callister, W. D.; Rethwisch, D. G. *Materials Science and Engineering: An Introduction*; Wiley: New York, 2007; Vol. 7.
(67) Kaltenbrunner, M.; White, M. S.; Glowacki, E. D.; Sekitani, T.; Someya, T.; Sariciftci, N. S.; Bauer, S. *Nat. Commun.* **2012**, *3*, 770.
(68) Oh, J. Y.; Shin, M.; Lee, T. I.; Jang, W. S.; Lee, Y. J.; Kim, C. S.; Kang, J. W.; Myoung, J. M.; Baik, H. K.; Jeong, U. *Macromolecules* **2013**, *46* (9), 3534−3543.
(69) Ito, Y.; Virkar, A. A.; Mannsfeld, S.; Oh, J. H.; Toney, M.; Locklin, J.; Bao, Z. A. *J. Am. Chem. Soc.* **2009**, *131* (26), 9396−9404.
(70) Schmidt, R.; Oh, J. H.; Sun, Y. S.; Deppisch, M.; Krause, A. M.; Radacki, K.; Braunschweig, H.; Konemann, M.; Erk, P.; Bao, Z. A.; Wurthner, F. *J. Am. Chem. Soc.* **2009**, *131* (17), 6215−6228.

DOI: 10.1021/acs.macromol.5b00524
Macromolecules 2015, 48, 4339−4346